ESC European Society of Cardiology

Cardiovascular Research (2024) **120**, 1164–1176
https://doi.org/10.1093/cvr/cvae104

FLT4 causes developmental disorders of the cardiovascular and lymphovascular systems via pleiotropic molecular mechanisms

Richard M. Monaghan [1]*, Richard W. Naylor [2], Daisy Flatman[3,4], Paul R. Kasher [3,4], Simon G. Williams [1], and Bernard D. Keavney [1,5]*

[1]Division of Cardiovascular Sciences, School of Medical Sciences, Faculty of Biology, Medicine, and Health, Manchester Academic Health Science Centre, University of Manchester, 5th Floor, AV Hill Building, Oxford Road, Manchester, M13 9NT, UK; [2]Wellcome Centre for Cell Matrix Research, Division of Cell Matrix Biology and Regenerative Medicine, School of Biological Sciences, Faculty of Biology, Medicine, and Health, Manchester Academic Health Science Centre, University of Manchester, Oxford Road, Manchester, M13 9PN, UK; [3]Division of Neuroscience and Experimental Psychology, School of Biological Sciences, University of Manchester, Oxford Road, Manchester, M13 9PT, UK; [4]Geoffrey Jefferson Brain Research Centre, Manchester Academic Health Science Centre, Northern Care Alliance NHS Foundation Trust, University of Manchester, Oxford Road, Manchester, M13 9PT, UK; and [5]Manchester Heart Institute, Manchester University NHS Foundation Trust, Oxford Road, M13 9WL, UK

Received 8 February 2023; revised 18 March 2024; accepted 19 March 2024; online publish-ahead-of-print 7 May 2024

Time for primary review: 69 days

Aims

Rare, deleterious genetic variants in *FLT4* are associated with Tetralogy of Fallot (TOF), the most common cyanotic congenital heart disease. The distinct genetic variants in *FLT4* are also an established cause of Milroy disease, the most prevalent form of primary hereditary lymphoedema. The phenotypic features of these two conditions are non-overlapping, implying pleiotropic cellular mechanisms during development.

Methods and results

In this study, we show that FLT4 variants identified in patients with TOF, when expressed in primary human endothelial cells, cause aggregation of FLT4 protein in the perinuclear endoplasmic reticulum, activating proteostatic and metabolic signalling, whereas lymphoedema-associated FLT4 variants and wild-type (WT) FLT4 do not. FLT4 TOF variants display characteristic gene expression profiles in key developmental signalling pathways, revealing a role for FLT4 in cardiogenesis distinct from its role in lymphatic development. Inhibition of proteostatic signalling abrogates these effects, identifying potential avenues for therapeutic intervention. Depletion of *flt4* in zebrafish caused cardiac phenotypes of reduced heart size and altered heart looping. These phenotypes were rescued with coinjection of WT human *FLT4* mRNA, but incompletely or not at all by mRNA harbouring *FLT4* TOF variants.

Conclusion

Taken together, we identify a pathogenic mechanism for FLT4 variants predisposing to TOF that is distinct from the known dominant negative mechanism of Milroy-causative variants. FLT4 variants give rise to conditions of the two circulatory subdivisions of the vascular system via distinct developmental pleiotropic molecular mechanisms.

* Corresponding authors. Tel: +44 161 306 3284, fax: +44 161 275 1183, E-mail: richard.monaghan@manchester.ac.uk (R.M.M.); Tel: +44 161 275 1225, fax: +44 161 275 1183, E-mail: bernard.keavney@manchester.ac.uk

Graphical Abstract

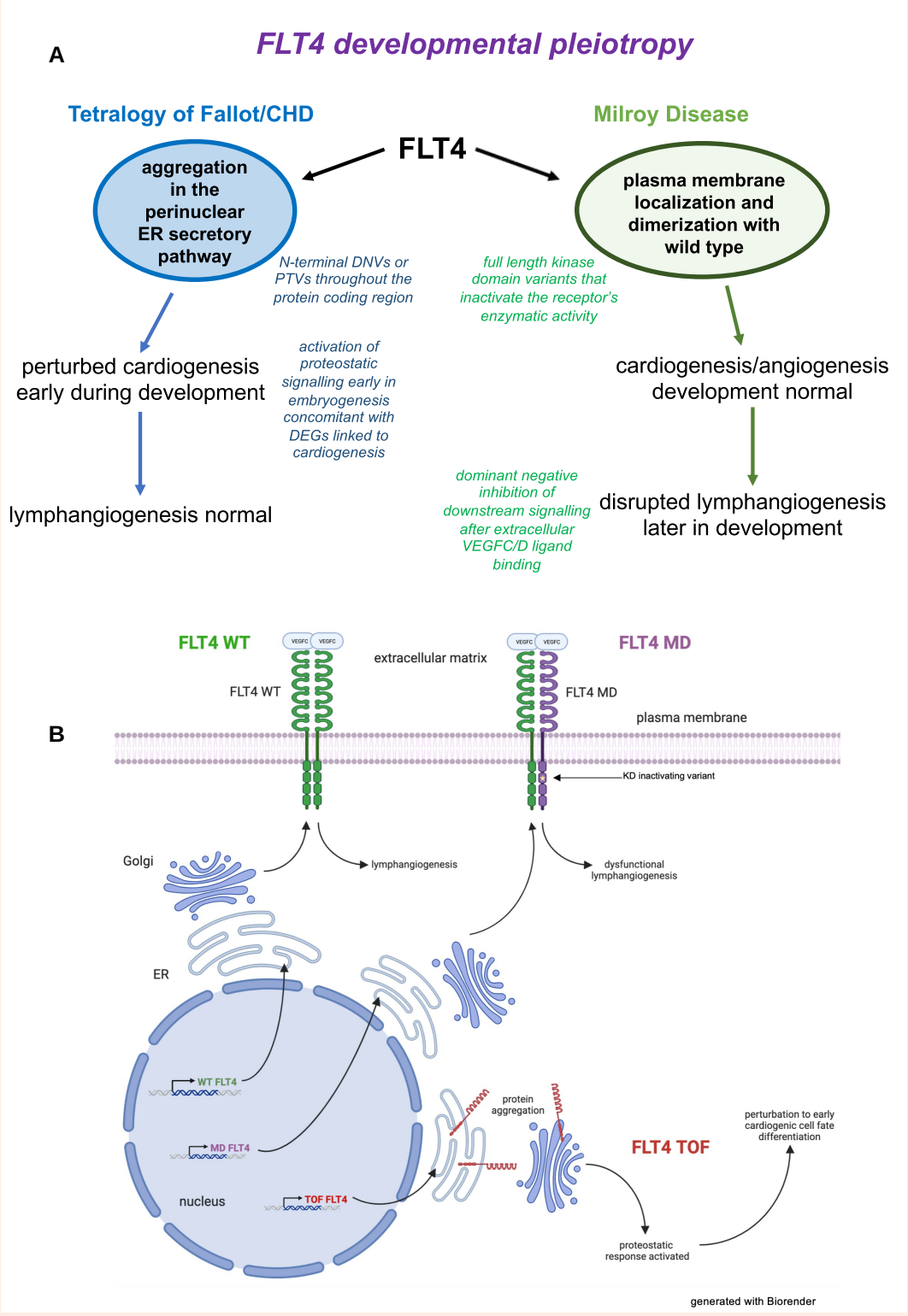

The differential subcellular localization of wild-type FLT4 , Milroy disease (MD), or Tetralogy of Fallot (TOF) variant, the subsequent downstream effects, and the predicted/characterized molecular mechanism of pathogenesis. (*A*) Graphical representation of FLT4 pleiotropy in TOF and MD. (*B*) Schematic representation of the cellular mechanism explicating the conclusions in (*A*).

Keywords Congenital heart disease • FLT4 • VEGFR3 • Developmental pleiotropy • Proteostasis • Primary lymphoedema • Tetralogy of Fallot

1. Introduction

Congenital heart disease (CHD) is the most common birth defect globally, identified in ~1% of newborns.[1,2] Large-scale sequencing of disease cohorts has identified predisposing genes in ~15% of such cases.[3,4] Sporadic, non-syndromic Tetralogy of Fallot (TOF) is the most common complex cyanotic CHD. Globally, multiple reports have independently identified rare deleterious genetic variants in *FLT4* (encoding vascular endothelial growth factor receptor 3, VEGFR3) in around 5% of non-syndromic patients with TOF using whole exome sequencing technology,[3,5–10] establishing it as one of the most significant individual genetic disease contributors. Although *FLT4* variants appear to predispose particularly to TOF, other clinical CHD phenotypes have also been described in patients reported to date.[9]

FLT4/VEGFR3 has established roles in lymphatic development and maintenance throughout life. Rare, dominant negative variants that abolish the receptor's kinase activity are an established cause of primary hereditary lymphoedema Type I, eponymously known as Milroy disease (MD). *FLT4* variants have been identified in ~60–70% of MD cases.[11,12] Mutant full-length FLT4 in MD heterodimerizes with wild-type (WT) FLT4 at the cell membrane upon extracellular ligand stimulation but prevents the activation of intracellular signalling due to the loss of transautophosphorylation. This leads to accelerated endocytic recycling of receptors to the plasma membrane (PM), resulting in the perturbation of lymphatic endothelial cell (EC) function and presentation of lymphoedema early in life.[11,12]

Neither TOF nor any other form of CHD is a phenotypic feature of MD, and conversely, lymphoedema is not a typical feature of sporadic, non-syndromic TOF. The *FLT4* variants that lead to the two conditions are distinct (*Figure 1*), indicating developmental pleiotropy (see Supplementary material online, *Figure S1*). MD is caused by heterozygous variants occurring almost exclusively in the kinase domain, whose activity they abolish. In contrast to MD, FLT4 genetic variants that predispose TOF are all heterozygous changes to date, and are either C-terminal protein-truncating variants (PTVs) or N-terminal missense variants predicted to be highly damaging to protein function.[4,13] Therefore, human genetic data indicate that *FLT4* exhibits non-overlapping pleiotropic actions, consequent on different classes of pathogenic variants.[14] These results are consistent with those observed in mouse models, where heterozygous *Flt4*$^{+/-}$ mice display normal angiogenesis but disrupted lymphangiogenesis,[13] and complete knockout of *Flt4* results in embryonic lethality at E9.5 owing to malformation of the heart.[15]

In this study, we aim to discover a cellular mechanism, whereby genetic variation in *FLT4* causes CHD. We demonstrate that different classes of FLT4 TOF variants aggregate in the perinuclear endoplasmic reticulum (ER)/vesicular secretory pathway, concomitant with activation of proteostatic, oxidative/reductive (redox), and mitochondrial homeostatic signalling. This behaviour is distinct from MD variants or WT FLT4. RNA sequencing (RNAseq) analysis of primary ECs expressing FLT4 variants shows a significant number of FLT4 TOF-specific differentially expressed genes (DEGs), compared with WT and MD. These genes significantly intersect with *in vivo* Stably expressed Heart development Genes (SHGs) and established human CHD genes. Both missense and PTV TOF-associated *FLT4* genetic changes act in a similar manner, through the same intracellular disease mechanism. Finally, early cardiogenic malformation phenotypes observed when endogenous zebrafish flt4 levels are significantly reduced and are rescued by coinjection of WT human *FLT4*, but not FLT4-TOF-truncating variants.

2. Methods

2.1 Cell lines, culture, maintenance, and expression of exogenous DNA

COS7, HEK293T, and HeLa cells were obtained from ATCC (Manassas, Virginia) and maintained at 37°C, 5% CO_2 in a humidified incubator; cultured in Dulbecco's modified Eagle's medium supplemented with 5 mM glutamine, 100 units mL^{-1} penicillin/streptomycin, and 10% foetal bovine serum (Life Technologies, Burlington, ON, Canada). Cells were transfected with Lipofectamine 3000 (L3000001, Thermo Fisher, Waltham, Massachusetts) following manufacturer's instructions.

Primary human umbilical vein ECs (HUVECs) pooled from four donors (lot number: 420Z015.1) were obtained from Promocell (C-12203). HUVECs were electroporated (see Supplementary Methods) with cell and DNA using a plastic Lonza disposable Pasteur pipette (for smaller well sizes the volumes were appropriately reduced).

2.2 DNA cloning, mutagenesis, and construct generation

pcDNA3.1-FLT4-V5 constructs were generated using the parent plasmid pcDNA3.1-VEGFR3 (FLT4 WT)-STREP, kindly provided by K. Alitalo (University of Helsinki); empty vector (EV) was pcDNA3.1. Deletions or insertions to generate FLT4 PTVs (TOF: 1-369*, 1-736*, 1-920*, 1-1036*) or introduction of the C-terminal V5 epitope tag was performed using Q5 Site-Directed Mutagenesis Kit (E0554, NEB,Ipswich, Massachusetts); FLT4-V5 point mutants (TOF: P30L, C51W; MD, G854S, R1041P; all single-nucleotide changes) were generated using QuikChange Lightning Multi Site-Directed Mutagenesis Kit (210516, Agilent, Cheadle, UK); manufacturer's instructions were followed for both kits and primer sequences are available on request.

2.3 Antibodies and costains

Primaries: mouse anti-ACTB (A2228, Sigma, Saint Louis, Missouri), rabbit anti-CANX (calnexin, Cell Signalling, 2433), mouse anti-FLAG (Sigma, F3165), anti-GM130 (D6B1) XP rabbit mAb (Cell Signalling), rabbit anti-histone 3 (H3, D1H2) XP rabbit mAb (Cell Signalling, Danvers, Massachusetts), rabbit anti- hypoxia inducible factor 1α (HIF1α; NB100-449, Novus Biologicals, Centennial, Colorado), rabbit anti-heat shock protein Family A, Member 5 (anti-HSPA5; BiP/GRP78, Cell Signalling, 3177), rabbit anti-Na^+/K^+ ATPase antibody (EP1845Y), and mouse anti-V5 (Thermo Fisher, R960). Secondaries: goat anti-mouse immunoglobulin G (IgG; H + L) poly-horseradish peroxidase (poly-HRP) secondary antibody (Thermo Fisher, 32230), goat anti-rabbit IgG (H + L) poly-HRP secondary antibody (Thermo Fisher, 32260), goat anti-rabbit IgG (H + L) cross-adsorbed secondary antibody, AlexaFluor 488 (Thermo Fisher, A-11008), goat anti-rabbit IgG (H + L) cross-adsorbed secondary antibody, AlexaFluor 594 (Thermo Fisher, A-11012), goat anti-mouse IgG (H + L) cross-adsorbed secondary antibody, AlexaFluor 488 (Thermo Fisher, A-11001), and goat anti-mouse IgG (H + L) highly cross-adsorbed secondary antibody, AlexaFluor 594 (Thermo Fisher, A-11032).

2.4 Immunofluorescence

Cells grown on glass coverslips, pre-coated with gelatin in the case of HUVECs, were washed twice with phosphate-buffered saline (PBS), then fixed at 20°C for 10 min in 4% formaldehyde, freshly prepared in PBS from a concentrated 36–38% formalin solution. Cells were then washed three times in PBS before blocking and permeabilization in 5% bovine serum albumin (BSA) and 0.01% Triton-X-100 in PBS for 45 min at 20°C (0.01% digitonin instead of Triton-X-100 was used for Na^+/K^+ exchanger-stained cells). Coverslips were incubated in primary antibodies for 18 h in fresh blocking buffer at 4°C, followed by four washes in PBS, before staining with secondary antibodies/costains in blocking buffer for an hour at 20°C, followed by a further four washes in PBS: all incubations and washes with mild agitation (see Supplementary Methods). PBS was aspirated and coverslips mounted onto glass slides with Vectorshield (H-1000-10, Vector Laboratories, Newark, California). Images were taken at 60xs objective using Olympus Microscopy Oil and an Olympus BX53 Microscope with DAPI (4′,6-diamidino-2-phenylindole), fluorescein isothiocyanate, and TxRed filters.

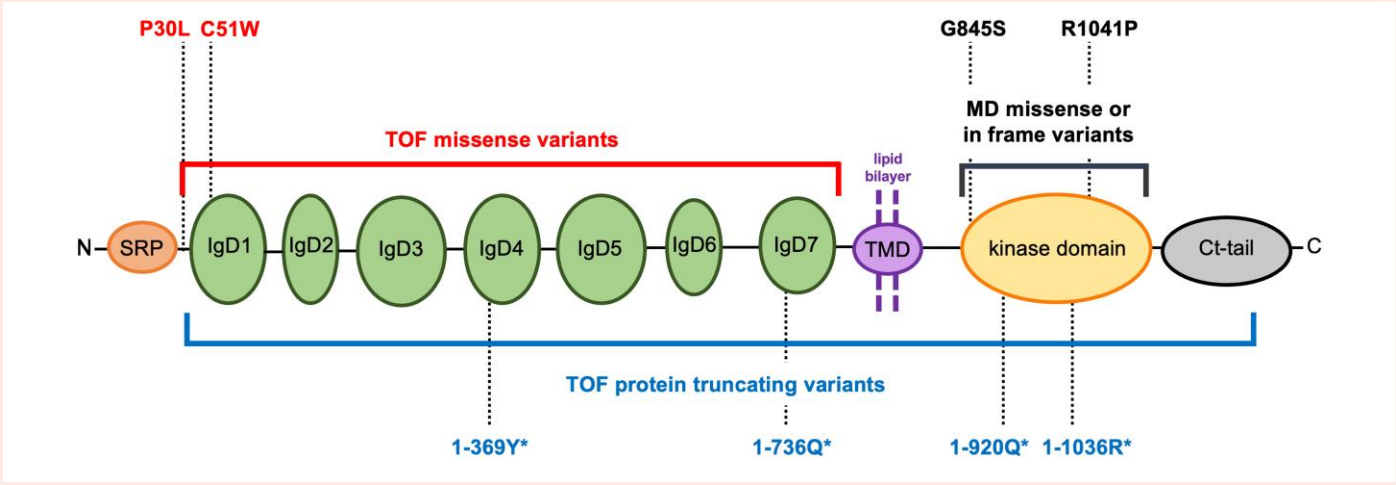

Figure 1 Schematic representation of FLT4/VEGFR3 protein. Red bracket: location of missense or in frame indels identified in TOF. Black bracket: location of inframe MD variants. Blue bracket: location of TOF-PTVs (P30fs*3 to Y1337fs*19). The eight variants experimentally studied here are indicated. SRP, signal recognition peptide; IgDs, immunoglobulin-like domains.

2.5 Immunoblotting

Immunoblotting was performed on cells washed in PBS and lysed and scraped in radio-immunoprecipitation assay buffer [25 mM pH 7.4 Tris-HCl, 150 mM NaCl, 1% IPEGAL (Sigma, I8896), 5 mM ethylenediaminetetraacetic acid, 0.1% sodium dodecyl sulphate (SDS), 1× protease inhibitor (Sigma, P2714)]. Followed by centrifugation at 14 000 *g* for 10 min. Supernatants were taken to new tubes and adjusted to 1× Laemmli Sample Buffer (Bio-Rad, 1610747) containing 355 mM 2-mercaptoethanol, samples were heated to 80°C for 5 min before being run on 4–20% Mini-PROTEAN TGX Precast Protein Gels (4561094, Bio-Rad, Hercules, California) using the Mini-PROTEAN system. Before transfer to nitrocellulose membranes using the pre-packed mini or midi electrophoresis kits and transfer system (Bio-Rad, for medium-sized proteins). Membranes were blocked in Tris-buffered saline and 0.1% Tween (TBST) with either 5% milk or BSA, for 1 h, before incubation overnight in the same buffer with primary antibodies. Membranes were washed five times in TBST before incubation in blocking buffer with secondary antibodies for 1 h at 20°C, before a further five washes in TBST. HRP-linked secondary antibody imaging was performed using Pierce reagents and blots captured on Kodak MR film.

2.6 Subcellular fractionation

Isolation of PM/cytoplasmic, organellar/secretory pathway or nuclear/nuclear-associated ER proteins from COS7 cells was performed effectively, as previously described (see Supplementary Methods). Each ~400 µL subcellular fraction was adjusted to 1× Laemmli Sample Buffer (Bio-Rad, 1610747) containing 355 mM 2-mercaptoethanol.

2.7 FLT4 minigene design, construction, and nonsense-mediated decay assay

An FLT4 intron-inclusion minigene (Exons 13–17), with an exogenous promoter and poly-A tail, an initiation start codon, in frame N- and C-terminal epitope tags, and a termination codon, was constructed using gDNA extracted from HUVECs (polymerase chain reactions (PCRs) 1–3) and the pcDNA3.1 parent plasmid (PCRs 4–6), using the NEBuilder HiFi DNA Assembly system (NEB, E2621S), following manufacturer's instructions (see Supplementary Methods). The Q736* single-nucleotide change was introduced using the QuikChange Lightning Multi Site-Directed Mutagenesis Kit (Agilent, 210516), following manufacturer's instructions. Primers for quantitative PCR (qPCR) of *FLT4* mRNA levels were upstream of the Q736* mutation and spanned exon–exon junctions. Primer sequences available on request.

2.8 RNA isolation, cDNA conversion, and qPCR

RNA was extracted from cells following one wash in PBS using the RNeasy Plus Mini Kit (Qiagen, Germantown, Maryland) following manufacturer's instructions. One microgram of RNA was converted to cDNA using the Applied Biosystems High-Capacity RNA-to-cDNA Kit, following manufacturer's instructions. qPCR was performed using Fast SYBR Green Master Mix (Thermo Fisher), following manufacturer's instructions. The ΔΔCt method was used to quantify gene expression changes with *ACTB* as the housekeeping gene, which is shown across all 12 FLT4 RNAseq samples as negligibly changed. Primer sequences were available on request.

2.9 RNA sequencing

RNAseq data were generated using standard protocols and bioinformatic analysis (see Supplementary Methods *S2.9* for complete experimental description).

2.10 Differential gene expression

We identified DEGs between WT and TOF variants, which were not differentially expressed between WT and MD. FLT4 WT RNAseq data were compared, using DESeq, successively with FLT4 MD, FLT4-TOF-PTV and FLT4-TOF-DNV. We designated as TOF-specific DEGs those that were significantly (adj. $P < 0.05$) differentially expressed in both the FLT4 WT vs. FLT4-TOF-DNV comparison, and the FLT4 WT vs. FLT4-TOF-PTV comparison, but not differentially expressed in the FLT4 WT vs. FLT4 MD comparison. These numbered 702 genes (see Supplementary material online, *Tables S1* and *S2*).

2.11 Inhibition of proteostatic signalling pathways

The three main pathways of proteostatic signalling were inhibited using small molecular chemical inhibitors applied to cell media following recovery from electroporation (see Supplementary Methods). IRE1α: 4μ8C (7-hydroxy-4-methyl-2-oxo-2H-1-benzopyran-8-carboxaldehyde, Sigma, 14003-96-4); PERK: GSK2606414 (7-methyl-5-(1-{[3-(trifluoromethyl) phenyl]acetyl}-2,3-dihydro-1H-indol-5-yl)-7H-pyrrolo[2,3-d]

pyrimidin-4-amine; A3448-APE, Stratech Scientific Ltd, St Thomas' Place, Ely, UK); ATP6: ceapin A7 (S. Nock, C. Gallagher, and P. Walter, UCSF).

2.12 *Danio rerio* husbandry, microinjection, time-lapse imaging, and *in situ* hybridization

Zebrafish were maintained and staged according to established protocols under project licence P1AE9A736 and within the current guidelines of the UK Animals Act 1986 (see Supplementary Methods for details). *FLT4* mRNA solution (WT, C51W, 1-736*, and 1-1036* mutant sequences) was diluted to 20.6 nM in RNase-free water. Five nanolitres of mRNA solution were injected directly into the cell of a one-cell-stage embryo using a microinjector to ensure equimolar amounts of mRNA were injected. Embryos were then transferred to E3 embryo medium and placed at 28.5°C until 48 h post-fertilization (hpf).

For primordial hindbrain channel (PHBC) imaging, injected and uninjected control *kdrl*:GFP zebrafish embryos were anaesthetized in buffered tricaine methanesulfonate (MS-222) at 164 mg L^{-1} at 48 hpf, before mounting in low melt agarose and imaged using light sheet microscopy, as previously described (see Supplementary Methods).

3. Results

3.1 FLT4 TOF variants aggregate in the perinuclear ER activating intracellular proteostatic signalling

Among accessible cell types potentially relevant to the aetiology of CHD, *FLT4* is expressed in vascular ECs during development, and its expression can be reinduced in these cells during angiogenesis. Primary HUVECs were therefore selected as the principal cell type for mechanistic investigations. Immunostaining of primary ECs, which under basal conditions exhibit low endogenous expression of FLT4,[16] expressing WT and MD FLT4 variants, demonstrated that they predominantly localized at the PM with a small proportion in the ER/vesicular pathway. This indicates that in our culture system, WT FLT4 and MD FLT4 variants are correctly processed and targeted to their main subcellular site of action, where they can bind their extracellular ligands. In contrast, FLT4 TOF variants, truncating or N-terminal missense, showed predominant staining of the perinuclear ER, or staining of both this pathway and only mild PM staining for transmembrane domain (TMD)-retaining PTVs (*Figure 2A* and *B*). Quantitative analysis in HeLa cells confirmed statistically significant differences in subcellular localization (see Supplementary material online, *Figure S2A and B*).

Subcellular localization results obtained by immunostaining were validated by differential fractionation of cells expressing FLT4 WT, MD, TOF-DNV, TOF-PTV (lacking a TMD), or TOF-PTV (retaining its TMD). A significant proportion of WT and MD FLT4 protein was observed in the PM/cytoplasmic fraction, less in the vesicular, and less in the nuclear fraction for WT, with the MD variant identified across all fractions (*Figure 2C*). In contrast, the three TOF variants examined—a DNV missense (C51W), a PTV without a TMD (1-736Q*), and a PTV retaining this domain (1-1036R*)—were strongly detected in the perinuclear ER only, with the PTV lacking a TMD (1-736Q*) also detected to a lesser degree in the other fractions (*Figure 2C*).

Given the aggregation of FLT4 TOF variants at the ER, alteration to proteostatic signalling was investigated in cells expressing FLT4 variants. Immunoblotting for HSPA5 (also known as GRP78 or BiP[17]), a marker of proteostatic signalling, was performed (*Figure 2G*). All FLT4 TOF variant expressing cells induced expression of HSPA5 significantly compared with those expressing WT, MD, or EV (quantitative analysis shown in *Figure 2H*). Thapsigargin, an inhibitor of the sarcoplasmic/ER Ca^{2+} ATPase served as a positive control.[18] The strongest effects were observed for the two FLT4 PTVs that lack TMDs and the two N-terminal missense variants. Proteostatic signalling by FLT4 TOF variants, both missense and protein truncating, was confirmed in primary human ECs by qPCR of key downstream genes of this response (*DDIT3/CHOP*[19] and *DNAJB9*,[20] *Figure 2E* and *F*, respectively).

3.2 Hypoxia mimetics stabilize FLT4-TOF-PTV mRNA and protein levels

In the early developing embryo, low oxygen levels play key signalling roles and their interaction with the nonsense-mediated decay (NMD) pathway has been shown to effect cell fate decisions.[21] To address the impact of NMD and/or C-degron[22] pathways on FLT4 PTVs, an intron-containing minigene reporter was designed and generated, as outlined in Supplementary material online, *Figure S4*. The minigene reporter was expressed in primary ECs either as WT or an FLT4-TOF-PTV-harbouring construct. Cells were then treated with two hypoxia mimetics that have distinctively different mechanisms of action. Dimethyloxallyl glycine (DMOG), a direct inhibitor of the HIF1α prolyl hydroxylase, stabilizing HIF1α protein levels;[23] or $CoCl_2$, a heavy metal transition ion that disrupts cellular redox status in a manner comparable with physiological hypoxia.[24] As observed in other cell types (see Supplementary material online, *Figure S4*), the FLT4 minigene reporters harbouring a PTV are expressed but at significantly lower levels than WT; however, both types of low-oxygen-simulating compounds significantly stabilize both RNA and protein levels of the N-terminally V5-tagged truncated peptide (*Figure 3A* and *B*, respectively). This indicates that conditions of low oxygen tension, such as those found in the early embryo, could allow for increased expression of *FLT4* harbouring PTVs and, therefore, amplify their pathogenic effects.[25–27]

3.3 Gene expression profiles of FLT4 variants in primary human ECs

We conducted RNAseq on primary human ECs expressing EV, FLT4 WT, MD, TOF-DNV, or TOF-PTV constructs. Expression of the FLT4-V5 constructs was assayed by immunoblot (see Supplementary material online, *Figure S5A*), confirming all constructs were expressed. Differential gene expression by 3D principal component analysis (PCA) analysis of all triplicate samples, including non-electroporated and EV expressing cells, showed sample replicates clustering together, and the TOF variant expressing cell transcriptomes clustering separately to the other samples (see Supplementary material online, *Figure S5B*). Significantly, DEGs for all pairwise comparisons are shown in Supplementary material online, *Table S1*. Of note, only 13 genes were differentially expressed between EV and FLT4 WT expressing cells (at adj. $P < 0.05$), indicating that primary EC biology is not markedly perturbed by ancillary expression of the WT receptor.

Figure 4A tabulates the numbers of DEGs between the different FLT4 construct expressing cells. Seven hundred and two significant (adj. $P < 0.05$) FLT4 TOF-specific DEGs were identified between cells expressing either type of TOF variant (DNV C51W or PTV 1-736*) and those expressing either WT or MD (R1041P) FLT4 (all genes listed in Supplementary material online, *Table S2*). Separating the 702 FLT4 TOF-specific DEGs into up- and down-regulated pathways, gene ontological (GO) enrichment analysis using Reactome[28] (*Figure 4B*, with individual gene names presented in Supplementary material online, *Table S3*) showed clustering of up-regulated genes in several pathways, including protein synthesis, PM targeting, RNA metabolism, mitochondrial metabolism (specifically oxidative phosphorylation/electron transport chain complexes), and developmental signalling pathways. Down-regulated genes showed less significant clustering; the only significant pathway (adj. $P < 0.05$) was chromatin organization, containing genes in which loss of function has been shown to be highly associated with CHD in multiple studies.[29]

The top 30% ($n = 5461$) of stably expressed heart developmental genes (SHGs) were identified across Mammalia (see Supplementary material online, *Table S4*, see Methods for the approach to their identification). Four hundred and forty-two (63%) of the 702 FLT4 TOF-specific DEGs are SHGs, compared with 30% expected by chance (permutation $P < 0.0001$). Forty-eight of the 702 FLT4 TOF-specific DEGs intersected

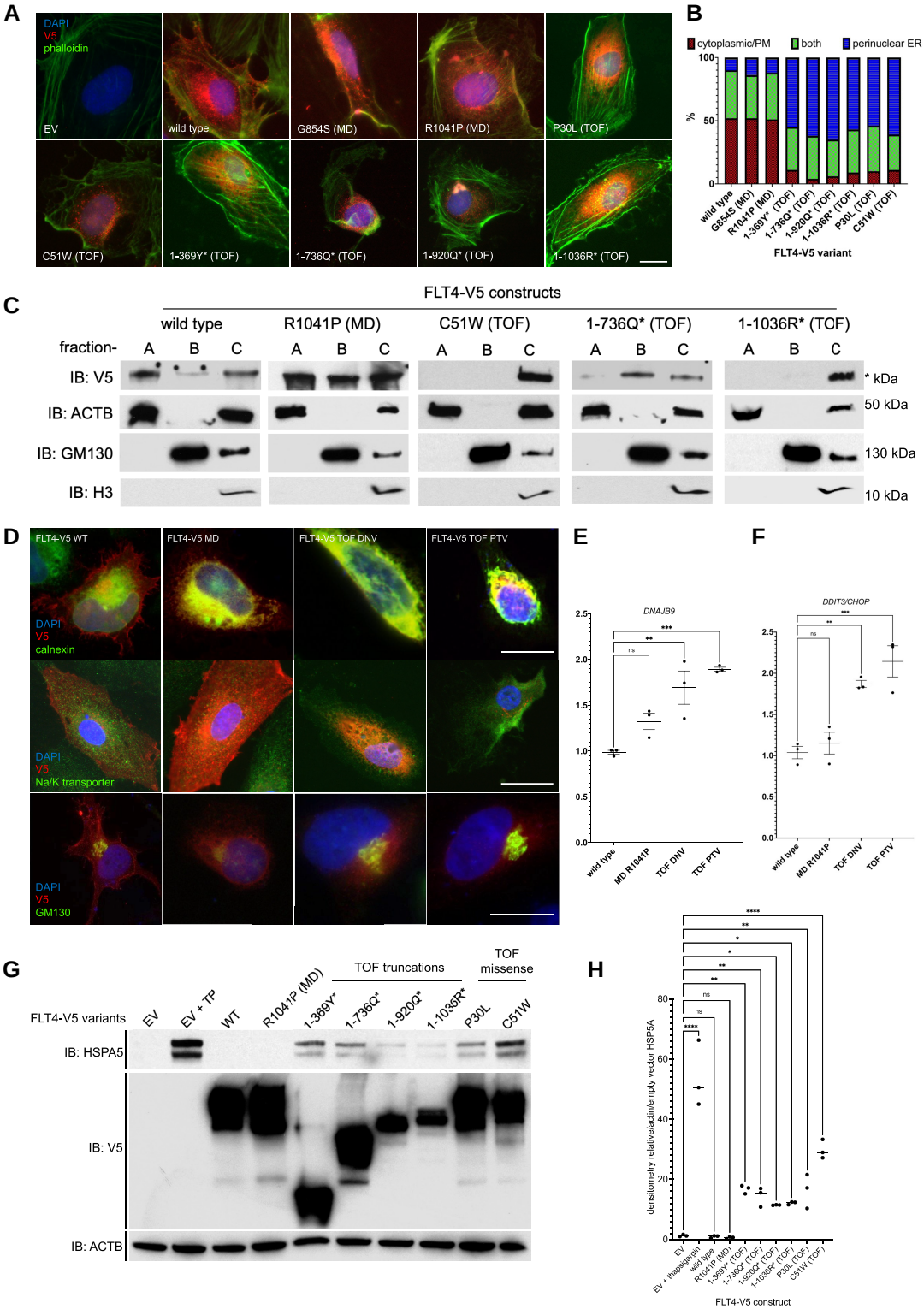

Figure 2 Subcellular localization and proteostatic signalling consequences of FLT4 TOF variants. (*A*) HUVECs expressing WT, MD, and TOF FLT4-V5 variants, stained with anti-V5 (red, FLT4), phalloidin (green, actin filaments), and DAPI (blue, nuclear stain). Scale bar, 10 μm. (*B*) Cells scored for three types of V5 staining, perinuclear/ER, PM/cytoplasmic, or both. One hundred cells in each group scored in each of three biological repeats. (*C*) Subcellular fractionation followed by immunoblotting for COS7 cells expressing FLT4 WT, MD, TOF-DNV, or two TOF-PTV variants. Fractions: A—PM, cytoplasmic; B—vesicular/Golgi apparatus-associated; or C—nuclear/perinuclear, ER. Markers: ACTB, cytoplasmic or nucleoplasmic cytoskeletal; GM130, Golgi apparatus; H3, histone 3, nuclear marker. V5-C-terminally tagged FLT4 variants. (*D*) Colocalization of FLT4-V5 tagged proteins with markers of the ER: calnexin; PM, Na/K-transporter; GM130, Golgi apparatus. (*E* and *F*) The activation of gene expression of proteostatic signalling by FLT4-TOF-DNV and FLT4-TOF-PTV variants. $n = 3$; $^{**}P < 0.01$; $^{***}P < 0.001$. (*G*) Activation of proteostatic signalling in HEK293T cells measured through HSP5A protein expression assessed by immunoblot. (*H*) Densiometric analysis of HSP5A bands relative to actin/EV from (*C*). $n = 3$, $^{*}P < 0.05$; $^{**}P < 0.01$, $^{****}P < 0.001$; one-way ANOVA compared with EV.

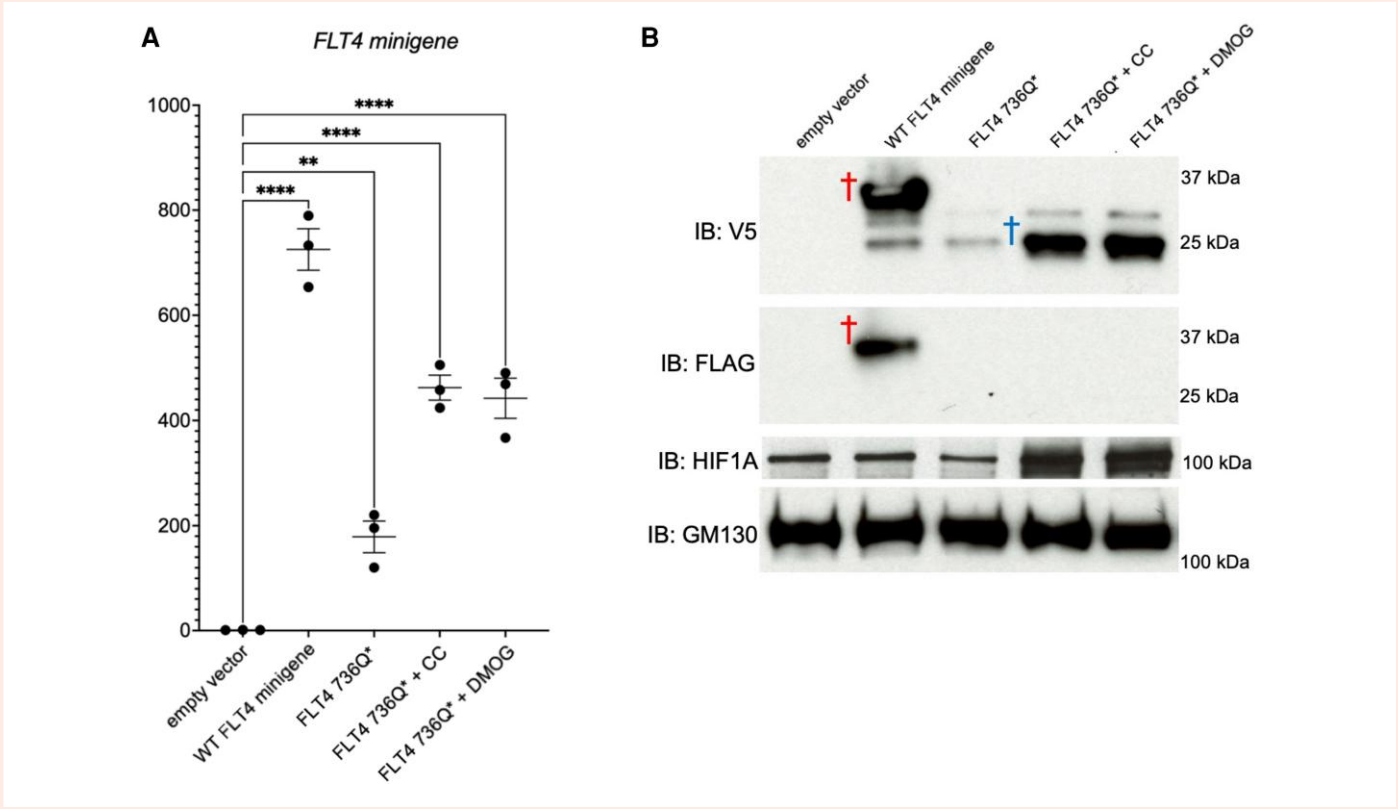

Figure 3 Hypoxia mimetics regulate the stability of an *FLT4*/ FLT4-TOF-PTV. RNA (*A*) or protein (*B*) was prepared from primary human ECs (HUVECs) expressing the FLT4 minigene assay construct (as outlined in Supplementary material online, *Figure S4*). EV, WT, or Q736* PTV FLT4 minigenes were untreated, or treated with the hypoxia mimetics, 0.2 mM cobalt chloride (CC) or 100 nM DMOG, for 3 h. Red dagger, full-length minigene protein, both V5 and FLAG positive; blue dagger, truncated minigene protein caused by the introduction of a nonsense codon and concomitant C-terminal cleavage, V5 positive only; $n = 3$; $^{**}P < 0.01$; $^{****}P < 0.0001$.

with a list of human CHD genes derived from three independent studies ($n = 716$, listed in Supplementary material online, *Table S5*, see Methods for the approach to their identification), approximately three-fold more than anticipated by chance (permutation $P < 0.0001$).

FLT4 TOF-specific DEGs were further analysed using IPA (Ingenuity Pathway Analysis, Qiagen) software. The top significant 'Diseases and Functions' (all $P < 0.02$) categories were *Congenital Heart Anomaly*, *Cardiac Hypoplasia*, and *Cardiac Stenosis*. *Figure 4C* displays the 702 DEGs from FLT4-TOF-specific variant expressing cells compared with WT and MD, as a volcano plot with mean log(Fold Change) and *P*-values derived from the PTV and DNV conditions. Genes taken forward for rescue analysis are labelled and those already associated with CHD in humans highlighted.

These results indicate that the two FLT4 TOF variants induce overlapping differential gene expression changes in a primary human endothelial precursor cell line that tie them directly to heart development/CHD. These are distinct from gene expression patterns in WT or MD FLT4 variant expressing cells, or cells carrying exogenous DNA (EV).

3.4 Inhibition of proteostatic signalling rescues FLT4-TOF-specific DEGs

We investigated whether chemical inhibition of proteostatic responses could rescue gene expression profiles in cells transfected with TOF variant constructs. Sixteen up-regulated and 16 down-regulated FLT4 TOF-specific DEGs were chosen using criteria outlined in Supplementary material online, *Table S6*. Selected genes (i) had a spread of significance/fold change, (ii) encompassed genes highlighted by GO analysis; or (iii) overlapped with human CHD, for example *KMT2A* and *NOTCH1* (*Figure 4C*). Differential expression of these 32 DEGs was first validated by qPCR in an additional set of triplicate experimental repeats (*Figure 5A* and *B*, Columns 1–4).

Inhibitors of the three major proteostatic signalling pathways, involving ATF6,[30,31] PERK,[32] and IRE1α,[33] were applied to cells directly following transfection and RNA extracted the following day. We first confirmed that the inhibitors were effective at suppressing known target genes of each pathway in our assay (see Supplementary material online, *Figure S6A–C*). Rescue of TOF-specific DEGs was observed for all three pathway inhibitors, as seen in *Figure 5*. IRE1α inhibition rescued the lowest number of gene expression changes (failure to rescue signified by crosses in the corresponding grid positions in *Figure 5*), while ATF6 inhibition rescued almost all gene expression changes, and PERK inhibition was intermediate between the two. Supplementary material online, *Figure S7A and B* show the complete qPCR results for all genes tested.

3.5 *In vivo* confirmation of a ligand binding-independent, dose-specific role, for FLT4 in early embryonic zebrafish heart development

We used the zebrafish (*D. rerio*) to provide *in vivo* evidence for differential function of *FLT4* TOF variants and WT *FLT4* in development. Previously, loss of *flt4* in zebrafish has been shown to abrogate formation of the PHBC, which are paired venous vessels running along the lateral walls of the hindbrain and draining into the anterior cardinal veins.[14] This validated phenotype was first used to gauge a concentration of WT human *FLT4* mRNA that is capable of rescuing *flt4*-depletion effects in zebrafish. Injection of a previously described[14] start codon-targeting flt4 MO into

A

DEGs adj. P<0.05	FLT4 TOF variant		
	C51W (DNV)	1-736Q* (PTV)	C51W and 1-736Q*
FLT4 WT	2011	4412	1628
FLT4 R1041P (MD)	1671	2026	943
FLT4 WT and R1041P	1028	1712	**702**

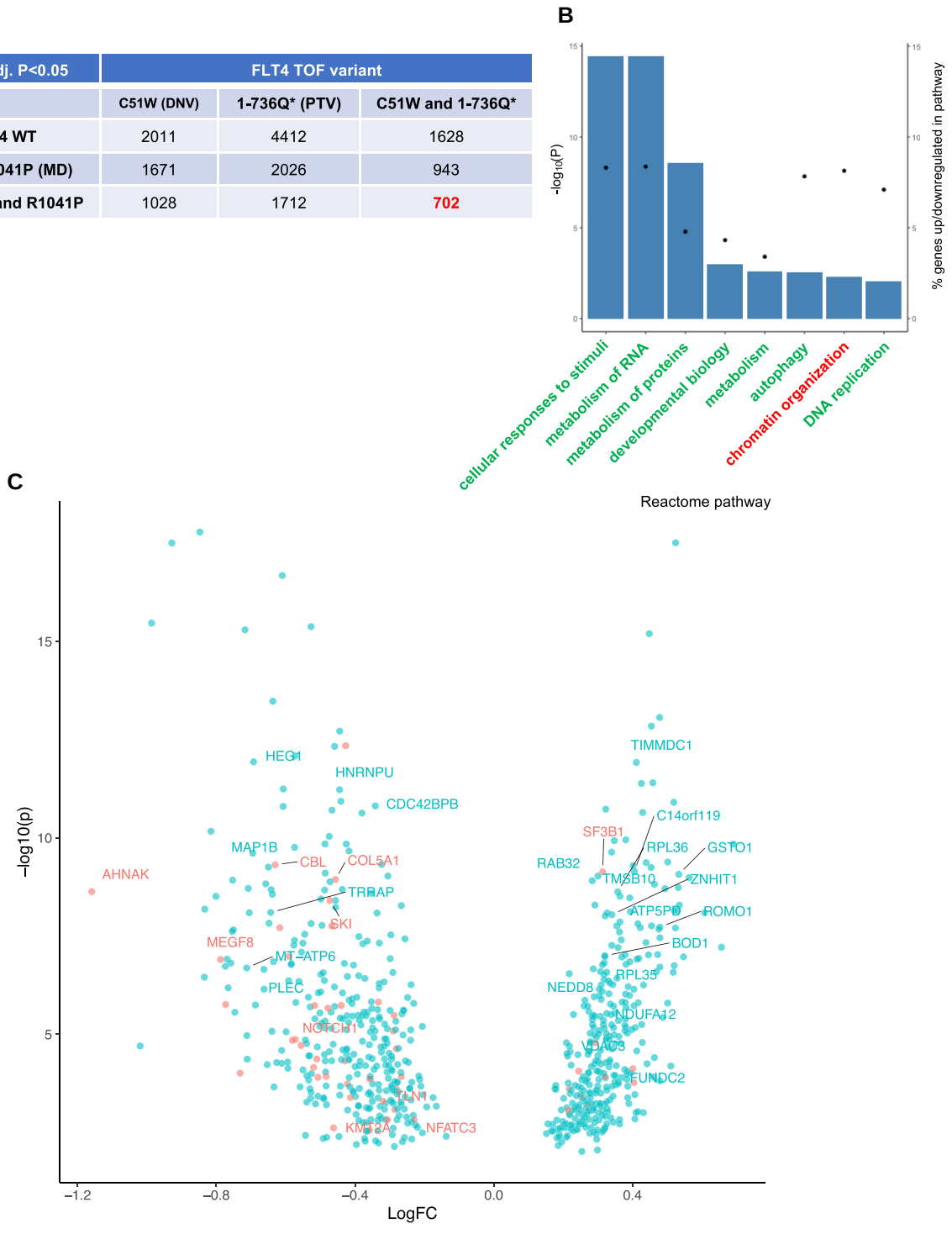

Figure 4 Distinct transcriptomic profiles of primary human ECs expressing both types of TOF variants compared with WT or an MD FLT4. (*A*) Distribution of DEGs between HUVECs expressing FLT4-V5 WT, FLT4 R1041P (MD), and FLT4 TOF-DNV (C51W) or FLT4-TOF-PTV (1-736Q*), identified by RNAseq. (*B*) Reactome analysis of the 702 TOF FLT4-specific DEGs, up- or down-regulated examined separately, displaying pathways identified with FDR < 0.01. (*C*) Volcano plot showing the 702 FLT4 TOF-specific DEGs, with genes taken forward for qPCR analysis labelled, and those previously associated with CHD in red.

WT zebrafish prevented PHBC formation in 37.9% of embryos (see Supplementary material online, *Figure S8A*). Injection of 125 pg FLT4 mRNA into flt4 morphants rescued PHBC formation, as only 7.4% of these embryos lacked a PHBC (see Supplementary material online, *Figure S8A*). In flt4 morphants injected with 250 pg WT FLT4 mRNA, 28.6% embryos had no PHBC. Similarly, 500 pg WT FLT4 mRNA co-injected into flt4 morphants caused absence of the PHBC in 32.1% of embryos. These results show 125 pg of FLT4 mRNA rescued flt4-depletion phenotypes most successfully, and hence, this dose was used in follow-up experiments. We therefore used 125 pg mRNA for follow-up experiments.

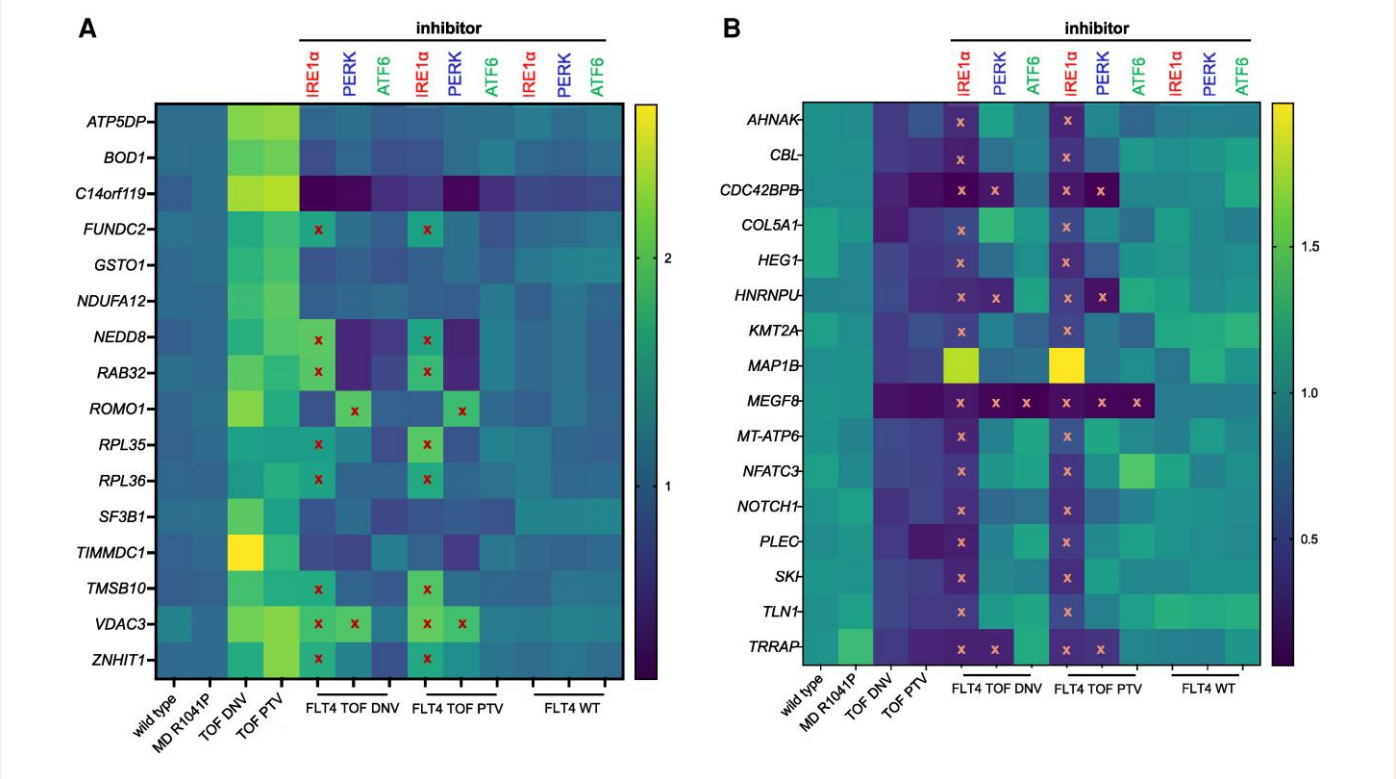

Figure 5 Rescue of FLT4 TOF-specific DEGs, represented as a heat map of gene expression levels, both (*A*) up-regulated and (*B*) down-regulated, by inhibitors of the three major proteostatic signalling pathways. Heat map of RNA levels (yellow highest, dark blue lowest) from HUVECs expressing WT FLT4-V5, MD, TOF-DNV, or TOF-PTV variants; the latter two treated with specific inhibitors of the three main proteostatic signalling pathways, or WT treated with the same inhibitors, above, IRE1α (red), PERK (blue), or ATF6 (green). Row names, gene targets. Red crosses represent no significant rescue (*P* still <0.05 compared with WT) and orange crosses represent DEGs whose expression changes not recused by drug treatment ($P < 0.05$ compared to WT still) of the gene expression changes induced by FLT4 TOF variant expression compared with WT.

To date, the presence of any cardiac phenotype in *flt4*-depleted zebrafish at 48 hpf has not been assessed. Injection of *flt4* MO into WT zebrafish caused a reduction in the size of the heart (*Figure 6A* and *B*; see Supplementary material online, *Figure S8B* for schematic of zebrafish embryo anatomy) and in heart looping (*Figure 6C*; see Supplementary material online, *Figure S8C* for description of heart looping phenotypes). These phenotypes were both rescued with 125 pg of *WT FLT4* mRNA. Neither heart looping nor cardiac size was rescued by coinjection of equimolar concentrations of 1-736* and 1-1036* *FLT4* mRNA. Heart looping was rescued by coinjection of the *FLT4 C51W* mRNA, but heart size remained significantly lower in *C51W* rescued animals than in those rescued by WT injection ($P < 0.05$, *Figure 6A–C*).

4. Discussion

Distinct variants in a single gene, *FLT4*, have previously been shown to lead to two non-overlapping congenital conditions, CHD (most significantly, TOF) and MD. We have demonstrated differences in molecular and cellular phenotypes between FLT4 variants found in patients with TOF and MD, outlining a potential mechanism for the developmental pleiotropy observed in previous human genetics studies. FLT4 TOF variants, of all types, subcellularly aggregated in the perinuclear/ER region of cells compared with WT or MD, activated proteostatic signalling, and resulted in downstream transcriptomic changes congruent with the development of CHD. Inhibition of the ATF6 and, to a lesser degree, PERK arms of the proteostatic response rescued expression of a panel of 32 FLT4 TOF-specific DEGs, indicating that it is most likely these pathways that mediate the observed gene expression changes. The overlap with murine SHGs and human CHD genes emphasizes the relevance of these results to the mechanism of disease pathology. In contrast with the already characterized FLT4 dominant negative kinase-inactivating variants that cause MD, our results suggest FLT4 TOF variants act through an incompletely penetrant, pathogenic mechanism, whereby the receptor's processing is disrupted, predisposing to the defects in cardiogenesis that lead to clinical disease.

FLT4 genetic variation has independently been shown by multiple groups to predispose to CHD, in particular TOF, but hitherto the mechanism of disease causation has been uncharacterized.[3–7,13,34] Since the dominant negative effect of MD variants on *FLT4* signalling does not cause a CHD phenotype, haploinsufficiency was *a priori* an unlikely causal explanation for disease in patients with TOF; this is congruent with the fact that haploinsufficient *Flt4* mice display lymphatic malformations but no CHD phenotype.[35,36] Additionally, we observe here that only low levels of human FLT4 mRNA is able to rescue the heart defects of zebrafish flt4 morphants, highlighting the dose requirement for the gene during cardiogenesis is lower than that required for lymphangiogenesis.

The latest version of the Genome Aggregation Database (v4.0; gnomAD)[37] contains information on FLT4 PTVs across >800K individuals (57 alleles, in 568 individuals). All PTVs currently listed are heterozygous, with very low allele frequencies, found only in one to three individuals, with the exception of the Y25* variant, identified in 492 individuals (see Supplementary material online, *Figure S9A and B*, and *Table S7*). Y25* has an allele frequency of ~0.0003, which is inconsistent with a role as a monogenic cause of TOF, which has a population prevalence of ~0.0005. However, presence of the Y25* allele would result in only the signal recognition peptide of the receptor (Residues 1–24) being encoded that would provide no substrate protein for the mechanism we have described. The higher allele frequency of Y25* in gnomAD adds

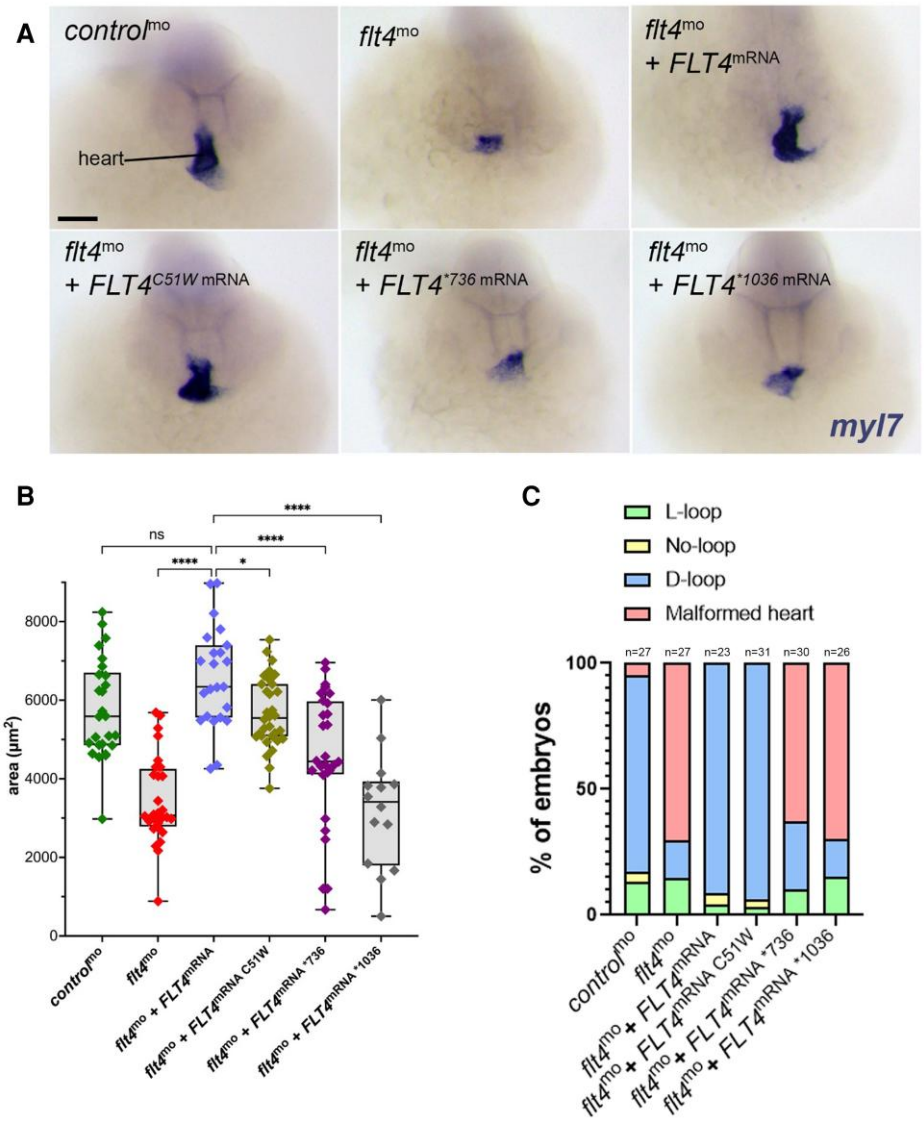

Figure 6 Rescue of zebrafish morphant cardiac phenotypes by *FLT4* variants. (*A*) Frontal views of 48 hpf embryos with *myl7* expression staining (purple) used to label the heart. (B) Box and whisker plot showing the area of embryonic hearts 48 hpf, taken from the co-injected *flt4* MO and *FLT4* variant mRNA samples. One-way ANOVA comparing all samples to the flt4-depleted MO sample rescued by co-injection of human *FLT4* expressing mRNA; *$P < 0.05$; ****$P < 0.0001$. (*C*) Histogram showing the percentage of embryos with d-loop, no loop/reduced heart size, or l-loop heart orientations.

further weight to the hypothesis that *FLT4* heterozygosity is tolerated, as copy number variant (CNV) studies have previously shown.[13] The FLT4 TOF-linked truncation P30fsR3*, which we and others have described, was identified in thirteen individuals in gnomAD, which would be consistent with an incompletely penetrant predisposing allele (MAF~8e−06).

This work demonstrates that FLT4 TOF variants act through a pathogenic mechanism whereby the receptor's posttranslational processing is disrupted; our findings that truncating variants escape NMD when treated with hypoxia mimetics suggest the possibility of gene–environment interactions that may be of importance in determining penetrance.[38–40] Examples of developmental pleiotropy in congenital diseases, as opposed to pleiotropy among inherited or somatic variants contributing to disease later in life, are sparse.[41–44] As an example, in the cardiovascular system, the *SCN5A* gene exhibits pleiotropy as a cause for Brugada syndrome, long-QT syndrome Type 3, dilated cardiomyopathy, and left ventricular non-compaction. However, we are unaware of previously identified pleiotropic genetic effects causing distinct, non-overlapping, conditions affecting the body's blood and lymphatic circulatory systems.[41]

The mechanism we propose here was common to both missense and protein-truncating FLT4 variants derived from patients with TOF. Examples of PTVs acting in a gain-of-function, novel, or augmented manner have previously been recognized in the literature. These include: pathological N- and C-terminal truncations of β-amyloid in dementia-associated plaques;[45] MN1 (meningioma 1, transcriptional activator) PTVs, which are a known cause of a recognizable syndrome with craniofacial and brain abnormalities;[46] mono- and biallelic PTVs in alpha-actinin 2, which cause cardiomyopathy through distinct gain-of-function (GoF) mechanisms;[47] and PTVs in SAMD9L (sterile alpha motif domain-containing 9 like), which cause B-cell aplasia and clinical autoinflammatory features through a heterozygous GoF mechanism.[38]

We showed that FLT4 TOF variants disrupted proteostatic mechanisms in cellular models. Disruption to proteostasis has been shown to lead to

higher incidence of CHD in mice when subjected to non-physiological gestational hypoxia, indicating it may be a common pathway whose dysregulation increases CHD occurrence.[39] Thus, our results on FLT4 CHD variants support those previous studies.[48] Intriguingly, vascular endothelial growth factor A signalling through VEGFR2 has been shown to activate ATF6-associated proteostatic responses, indicative of a connection between these two signalling pathways independent of proteostatic stress. Genes involved in cysteine-dependent ER redox homeostasis, posttranslational modification of proteins such as glycosylation, and entry to the secretory pathway that leads nascent polypeptides to the PM, are enriched in FLT4 TOF-specific DEGs and are directly linked to proteostatic responses from the organelle, and foetal growth restriction in mice.[1,49–55]

The *FLT4* locus is highly conserved. Previous studies have demonstrated an essential role for *flt4* in zebrafish angiogenesis and cardiac valvulogenesis.[56] We found heart development is significantly perturbed in zebrafish *flt4* morphants. Neither the 1-736* or 1-1036* FLT4 PTVs were able to rescue *flt4*-depletion cardiac phenotypes. The human FLT4 TOF variant C51W was able to rescue heart looping comparably with WT *FLT4* in *flt4*-depleted embryos and to a significantly lesser degree, the reduced heart area phenotype. This may be accounted for by the fact that the C111 residue at the other end of the disulphide bridge to which the highly conserved C51 residue contributes, is not conserved in zebrafish,[57] lessening the impact of the C51W variant in the fish.

Our data suggest that inhibitors of the proteostatic response, particularly, ceapin A7 (ATF6 inhibitor, which prevents cleavage and nuclear translocation of ATF6's transcriptional activation domain at the Golgi apparatus) may merit further investigation as modulators of CHD risk.[30,49] If the proteostatic responses were shown to be a global CHD mechanism, common to several genetic aetiologies, there could be a therapeutic opportunity to prevent disease in high risk families. The use of IRE1α inhibitors in a murine model of Kawasaki disease alleviates phenotypic features,[58,59] giving credence to the hypothesis that targeting the proteostatic response could be a route to clinical intervention. The significant enrichment of mitochondrial metabolic genes in FLT4 TOF-specific DEGs is intriguing since targeting mitochondrial dysfunction, specifically in cases of cyanotic CHD, has been postulated as a potential therapeutic goal.[60,61] Technologies capable of overriding specific nonsense mutations have also recently been described.[62,63] This work supports that of others indicating that gestational hypoxia coupled with genetic variation, acting through disrupted proteostasis, could be a common phenomenon in CHD pathogenesis.[39,40]

This work has some limitations. HUVECs are not a developmental cell line, and confirmation of these findings in cells of endocardial lineage differentiated from human embryonic stem cells[64–66] would be of considerable interest. Future work, modelling specific human TOF FLT4 variants in the mouse in selected developmental lineages, will likely yield further insights into the anatomical aspects of their action.

The postnatal consequences of the cellular processes we have identified to be disrupted by FLT4 TOF variants remain uncertain. Recent large-scale epidemiological data from the UK Biobank show that patients with CHD have important predispositions to later life comorbidities, including coronary artery disease[67] and chronic obstructive pulmonary disease,[68] for unknown reasons. Whether genetic predisposition to altered proteostasis implicated in CHD risk could also impact CHD-associated comorbidities later in life also requires investigation.

Translational perspective

Proteostatic dysfunction, if confirmed as a mechanism of congenital heart disease (CHD) pathogenesis for other predisposing genes, may identify pathways to therapeutic interventions. Distinguishing mechanistically how variants in *FLT4* give rise to CHD may aid in individualizing genetic counselling in affected families.

Supplementary material

Supplementary material is available at *Cardiovascular Research* online.

Authors' contributions

Conceived and designed the study: R.M.M., R.W.N., P.R.K., and B.D.K. Performed experiments and analysed data: R.M.M., R.W.N., D.F., and S.G.W. Wrote paper: R.M.M., R.W.N., P.R.K., and B.D.K. Handled supervision and funding: P.R.K. and B.D.K. Revised and edited paper for critical intellectual content: all authors.

Acknowledgements

From the University of Manchester, the authors thank the Genomic Technologies Core Facility for undertaking the RNAseq experiments, Alan Whitmarsh for his analytical reading of the manuscript, and Professor Rachel Lennon for support of the zebrafish work. The authors also thank the Bioimaging Core Facility for access to microscopes and the Biological Support Facility for zebrafish husbandry.

Conflict of interest: none declared.

Funding

Supported by a British Heart Foundation (BHF) Personal Chair (CH/13/2/30154) and BHF Programme Grant (RG/F/21/110050) and by the National Institute of Health Research Manchester Biomedical Research Centre. R.W.N. supported by a Kidney Research UK, Intermediate Fellowship (INT_009_20191202). P.R.K. supported by the Medical Research Council (UK) (MR/T03291X/1). D.F. was funded by a BHF 4-year PhD grant (FS/4yPhD/F/20/34131).

Data availability

Raw data are available through the GEO data set: GSE204910. The primer sequences for cloning and qPCR data are available from the corresponding authors upon request.

References

1. Yi K, Xu JG, Yang KL, Zhang X, Ma L, You T, Tian JH. The top-100 most cited articles of biomarkers in congenital heart disease: a bibliometric analysis. *Ann Palliat Med* 2022;**11**:1700–1713.
2. Liu Y, Chen S, Zuhlke L, Black GC, Choy MK, Li N, Keavney BD. Global birth prevalence of congenital heart defects 1970-2017: updated systematic review and meta-analysis of 260 studies. *Int J Epidemiol* 2019;**48**:455–463.
3. Jin SC, Homsy J, Zaidi S, Lu Q, Morton S, DePalma SR, Zeng X, Qi H, Chang W, Sierant MC, Hung W-C, Haider S, Zhang J, Knight J, Bjornson RD, Castaldi C, Tikhonoa IR, Bilguvar K, Mane SM, Sanders SJ, Mital S, Russell MW, Gaynor JW, Deanfield J, Giardini A, Porter GA, Srivastava D, Lo CW, Shen Y, Watkins WS, Yandell M, Yost HJ, Tristani-Firouzi M, Newburger JW, Roberts AE, Kim R, Zhao H, Kaltman JR, Goldmuntz E, Chung WK, Seidman JG, Gelb BD, Seidman CE, Lifton RP, Brueckner M. Contribution of rare inherited and de novo variants in 2,871 congenital heart disease probands. *Nat Genet* 2017;**49**:1593–1601.
4. Page DJ, Miossec MJ, Williams SG, Monaghan RM, Fotiou E, Cordell HJ, Sutcliffe L, Topf A, Bourgey M, Bourque G, Eveleigh R, Dunwoodie SL, Winlaw DS, Bhattacharya S, Breckpot J, Devriendt K, Gewillig M, Brook JD, Setchfield KJ, Bu'Lock FA, O'Sullivan J, Stuart G, Bezzina CR, Mulder BJM, Postma Alex V., Bentham James R., Baron Martin, Bhaskar Sanjeev S., Black Graeme C., Newman William G., Hentges Kathryn E., Lathrop G. Mark, Santibanez-Koref Mauro, Keavney Bernard D. Whole exome sequencing reveals the major genetic contributors to nonsyndromic tetralogy of Fallot. *Circ Res* 2019;**124**:553–563.
5. Homsy J, Zaidi S, Shen YF, Ware JS, Samocha KE, Karczewski KJ, DePalma SR, McKean D, Wakimoto H, Gorham J, Jin SC, Deanfield J, Giardini A, Porter GA, Kim R, Bilguvar K,

López-Giráldez F, Tikhonova I, Mane S, Romano-Adesman A, Qi H, Vardarajan B, Ma L, Daly M, Roberts AE, Russell MW, Mital S, Newburger JW, Gaynor JW, Breitbart RE, Iossifov I, Ronemus M, Sanders SJ, Kaltman JR, Seidman JG, Brueckner M, Gelb BD, Goldmuntz E, Lifton RP, Seidman CE, Chung WK. De novo mutations in congenital heart disease with neurodevelopmental and other congenital anomalies. *Science* 2015;**350**:1262–1266.

6. Szot JO, Cuny H, Blue GM, Humphreys DT, Ip E, Harrison K, Sholler GF, Giannoulatou E, Leo P, Duncan EL, Sparrow DB, Ho JWK, Graham RM, Pachter N, Chapman G, Winlaw DS. A screening approach to identify clinically actionable variants causing congenital heart disease in exome data. *Circ Genom Precis Med* 2018;**11**:e001978.
7. Reuter MS, Jobling R, Chaturvedi RR, Manshaei R, Costain G, Heung T, Curtis M, Hosseini SM, Liston E, Lowther C, Oechslin E, Sticht H, Thiruvahindrapuram B, van Mil S, Wald RM, Walker S, Marshall CR, Silversides CK, Scherer SW, Kim RH, Bassett AS. Haploinsufficiency of vascular endothelial growth factor related signaling genes is associated with tetralogy of Fallot. *Genet Med* 2019;**21**:1001–1007.
8. Sevim Bayrak C, Zhang P, Tristani-Firouzi M, Gelb BD, Itan Y. De novo variants in exomes of congenital heart disease patients identify risk genes and pathways. *Genome Med* 2020;**12**:9.
9. Tabib A, Talebi T, Ghasemi S, Pourirahim M, Naderi N, Maleki M, Kalayinia S. A novel stop-gain pathogenic variant in FLT4 and a nonsynonymous pathogenic variant in PTPN11 associated with congenital heart defects. *Eur J Med Res* 2022;**27**:286.
10. Reuter MS, Chaturvedi RR, Liston E, Manshaei R, Aul RB, Bowdin S, Cohn I, Curtis M, Dhir P, Hayeems RZ, Hosseini SM, Khan R, Ly LG, Marshall CR, Mertens L, Okello JBA, Pereira SL, Raajkumar A, Seed M, Thiruvahindrapuram B, Scherer SW, Kim RH, Jobling RK. The Cardiac Genome Clinic: implementing genome sequencing in pediatric heart disease. *Genet Med* 2020;**22**:1015–1024.
11. Gordon K, Varney R, Keeley V, Riches K, Jeffery S, Van Zanten M, Mortimer P, Ostergaard P, Mansour S. Update and audit of the St George's classification algorithm of primary lymphatic anomalies: a clinical and molecular approach to diagnosis. *J Med Genet* 2020;**57**:653–659.
12. Karkkainen MJ, Ferrell RE, Lawrence EC, Kimak MA, Levinson KL, McTigue MA, Alitalo K, Finegold DN. Missense mutations interfere with VEGFR-3 signalling in primary lymphoedema. *Nat Genet* 2000;**25**:153–159.
13. Monaghan RM, Page DJ, Ostergaard P, Keavney BD. The physiological and pathological functions of VEGFR3 in cardiac and lymphatic development and related diseases. *Cardiovasc Res* 2021;**117**:1877–1890.
14. Hogan BM, Herpers R, Witte M, Helotera H, Alitalo K, Duckers HJ, Schulte-Merker S. Vegfc/Flt4 signalling is suppressed by Dll4 in developing zebrafish intersegmental arteries. *Development* 2009;**136**:4001–4009.
15. Dumont DJ, Jussila L, Taipale J, Lymboussaki A, Mustonen T, Pajusola K, Breitman M, Alitalo K. Cardiovascular failure in mouse embryos deficient in VEGF receptor-3. *Science* 1998;**282**:946–949.
16. Schumacher JA, Wright ZA, Owen ML, Bredemeier NO, Sumanas S. Integrin alpha5 and Integrin alpha4 cooperate to promote endocardial differentiation and heart morphogenesis. *Dev Biol* 2020;**465**:46–57.
17. Booth L, Roberts JL, Cash DR, Tavallai S, Jean S, Fidanza A, Cruz-Luna T, Siembiba P, Cycon KA, Cornelissen CN, Dent P. GRP78/BiP/HSPA5/Dna k is a universal therapeutic target for human disease. *J Cell Physiol* 2015;**230**:1661–1676.
18. Ball M, Andrews SP, Wierschem F, Cleator E, Smith MD, Ley SV. Total synthesis of thapsigargin, a potent SERCA pump inhibitor. *Org Lett* 2007;**9**:663–666.
19. Jauhiainen A, Thomsen C, Strombom L, Grundevik P, Andersson C, Danielsson A, Andersson MK, Nerman O, Rorkvist L, Stahlberg A, Åman P. Distinct cytoplasmic and nuclear functions of the stress induced protein DDIT3/CHOP/GADD153. *PLoS One* 2012;**7**:e33208.
20. Lee HJ, Kim JM, Kim KH, Heo JI, Kwak SJ, Han JA. Genotoxic stress/p53-induced DNAJB9 inhibits the pro-apoptotic function of p53. *Cell Death Differ* 2015;**22**:86–95.
21. Lou CH, Chousal J, Goetz A, Shum EY, Brafman D, Liao X, Mora-Castilla S, Ramaiah M, Cook-Andersen H, Laurent L, Wilkinson MF. Nonsense-mediated RNA decay influences human embryonic stem cell fate. *Stem Cell Reports* 2016;**6**:844–857.
22. Makaros Y, Raiff A, Timms RT, Wagh AR, Gueta MI, Bekturova A, Guez-Haddad J, Brodsky S, Opatowsky Y, Glickman MH, Elledge SJ, Koren I. Ubiquitin-independent proteasomal degradation driven by C-degron pathways. *Mol Cell* 2023;**83**:1921–1935 e1927.
23. Yuan Q, Bleiziffer O, Boos AM, Sun J, Brandl A, Beier JP, Arkudas A, Schmitz M, Kneser U, Horch RE. PHDs inhibitor DMOG promotes the vascularization process in the AV loop by HIF-1a up-regulation and the preliminary discussion on its kinetics in rat. *BMC Biotechnol* 2014;**14**:112.
24. Sandner P, Wolf K, Bergmaier U, Gess B, Kurtz A. Hypoxia and cobalt stimulate vascular endothelial growth factor receptor gene expression in rats. *Pflugers Arch* 1997;**433**:803–808.
25. Goetz AE, Wilkinson M. Stress and the nonsense-mediated RNA decay pathway. *Cell Mol Life Sci* 2017;**74**:3509–3531.
26. Zhao Y, Kang X, Gao F, Guzman A, Lau RP, Biniwale R, Wadehra M, Reemtsen B, Garg M, Halnon N, Quintero-Rivera F, Van Arsdell G, Coppola G, Nelson SF, Touma M, Touma M, Halnon N, Reemtsen B, Alejos J, Biniwale R, Federman M, Reardon L, Garg M, Speirs A, Finn JP, Quintero-Rivera F, Grody W, Van Arsdell G, Nelson S, Wang Y. Gene-environment regulatory circuits of right ventricular pathology in tetralogy of Fallot. *J Mol Med (Berl)* 2019;**97**:1711–1722.
27. Bartoszewska S, Collawn JF. Unfolded protein response (UPR) integrated signaling networks determine cell fate during hypoxia. *Cell Mol Biol Lett* 2020;**25**:18.
28. Gillespie M, Jassal B, Stephan R, Milacic M, Rothfels K, Senff-Ribeiro A, Griss J, Sevilla C, Matthews L, Gong C, Deng C, Varusai T, Ragueneau E, Haider Y, May B, Shamovsky V, Weiser J, Brunson T, Sanati N, Beckman L, Shao X, Fabregat A, Sidiropoulos K, Murillo J, Viteri G, Cook J, Shorser S, Bader G, Demir E, Sander C, Haw R, Wu G, Stein L, Hermjakob H, D'Eustachio P. The reactome pathway knowledgebase 2022. *Nucleic Acids Res* 2022;**50**:D687–D692.
29. Zaidi S, Choi M, Wakimoto H, Ma L, Jiang J, Overton JD, Romano-Adesman A, Bjornson RD, Breitbart RE, Brown KK, Carriero NJ, Cheung YH, Deanfield J, DePalma S, Fakhro KA, Glessner J, Hakonarson H, Italia MJ, Kaltman JR, Kaski J, Kim R, Kline JK, Lee T, Leipzig J, Lopez A, Mane SM, Mitchell LE, Newburger JW, Parfenov M, Pe'er I, Porter G, Roberts AE, Sachidanandam R, Sanders SJ, Seiden HS, State MW, Subramanian S, Tikhonova IR, Wang W, Warburton D, White PS, Williams IA, Zhao H, Seidman JG, Brueckner M, Chung WK, Gelb BD, Goldmuntz E, Seidman CE, Lifton RP. De novo mutations in histone-modifying genes in congenital heart disease. *Nature* 2013;**498**:220–223.
30. Torres SE, Gallagher CM, Plate L, Gupta M, Liem CR, Guo X, Tian R, Stroud RM, Kampmann M, Weissman JS, Walter P. Ceapins block the unfolded protein response sensor ATF6alpha by inducing a neomorphic inter-organelle tether. *Elife* 2019;**8**:e46595.
31. Ma M, Li H, Wang P, Yang W, Mi R, Zhuang J, Jiang Y, Lu Y, Shen X, Wu Y, Shen H. ATF6 aggravates angiogenesis-osteogenesis coupling during ankylosing spondylitis by mediating FGF2 expression in chondrocytes. *iScience* 2021;**24**:102791.
32. Sun J, Chen W, Li S, Yang S, Zhang Y, Hu X, Qiu H, Wu J, Xu S, Chu T. Nox4 promotes RANKL-induced autophagy and osteoclastogenesis via activating ROS/PERK/eIF-2alpha/ATF4 pathway. *Front Pharmacol* 2021;**12**:751845.
33. Cross BC, Bond PJ, Sadowski PG, Jha BK, Zak J, Goodman JM, Silverman RH, Neubert TA, Baxendale IR, Ron D, Harding HP. The molecular basis for selective inhibition of unconventional mRNA splicing by an IRE1-binding small molecule. *Proc Natl Acad Sci U S A* 2012;**109**:E869–E878.
34. Choudhury TZ, Garg V. Molecular genetic mechanisms of congenital heart disease. *Curr Opin Genet Dev* 2022;**75**:101949.
35. Diab NS, Barish S, Dong W, Zhao S, Allington G, Yu X, Kahle KT, Brueckner M, Jin SC. Molecular genetics and complex inheritance of congenital heart disease. *Genes (Basel)* 2021;**12**:1020.
36. Irrthum A, Karkkainen MJ, Devriendt K, Alitalo K, Vikkula M. Congenital hereditary lymphedema caused by a mutation that inactivates VEGFR3 tyrosine kinase. *Am J Hum Genet* 2000;**67**:295–301.
37. Karczewski KJ, Francioli LC, Tiao G, Cummings BB, Alfoldi J, Wang Q, Collins RL, Laricchia KM, Ganna A, Birnbaum DP, Gauthier LD, Brand H, Solomonson M, Watts NA, Rhodes D, Singer-Berk M, England EM, Seaby EG, Kosmicki JA, Walters RK, Tashman K, Farjoun Y, Banks E, Poterba T, Wang A, Seed C, Whiffin N, Chong JX, Samocha KE, Pierce-Hoffman E, Zappala Z, O'Donnell-Luria AH, Minikel EV, Weisburd B, Lek M, Ware JS, Vittal C, Armean IM, Bergelson L, Cibulskis K, Connolly KM, Covarrubias M, Donnelly S, Ferriera S, Gabriel S, Gentry J, Gupta N, Jeandet T, Kaplan D, Llanwarne C, Munshi R, Novod S, Petrillo N, Roazen D, Ruano-Rubio V, Saltzman A, Schleicher M, Soto J, Tibbetts K, Tolonen C, Wade G, Talkowski ME, Aguilar Salinas CA, Ahmad T, Albert CM, Ardissino D, Atzmon G, Barnard J, Beaugerie L, Benjamin EJ, Boehnke M, Bonnycastle LL, Bottinger EP, Bowden DW, Bown MJ, Chambers JC, Chan JC, Chasman D, Cho J, Chung MK, Cohen B, Correa A, Dabelea D, Daly MJ, Darbar D, Duggirala R, Dupuis J, Ellinor PT, Elosua R, Erdmann J, Esko T, Färkkilä M, Florez J, Franke A, Getz G, Glaser B, Glatt SJ, Goldstein D, Gonzalez C, Groop L, Haiman C, Hanis C, Harms M, Hiltunen M, Holi MM, Hultman CM, Kallela M, Kaprio J, Kathiresan S, Kim B-J, Kim YJ, Kirov G, Kooner J, Koskinen S, Krumholz HM, Kugathasan S, Kwak SH, Laakso M, Lehtimäki T, Loos RJF, Lubitz SA, Ma RCW, MacArthur DG, Marrugat J, Mattila KM, McCarroll S, McCarthy MI, McGovern D, McPherson R, Meigs JB, Melander O, Metspalu A, Neale BM, Nilsson PM, O'Donovan MC, Ongur D, Orozco L, Owen MJ, Palmer CNA, Palotie A, Park KS, Pato C, Pulver AE, Rahman N, Remes AM, Rioux JD, Ripatti S, Roden DM, Saleheen D, Salomaa V, Samani NJ, Scharf J, Schunkert H, Shoemaker MB, Sklar P, Soininen H, Sokol H, Spector T, Sullivan PF, Suvisaari J, Tai ES, Teo YY, Tiinamaija T, Tsuang M, Turner D, Tusie-Luna T, Vartiainen E, Vawter MP, Ware JS, Watkins H, Weersma RK, Wessman M, Wilson JG, Xavier RJ, Neale BM, Daly MJ, MacArthur DG. The mutational constraint spectrum quantified from variation in 141,456 humans. *Nature* 2020;**581**:434–443.
38. Allenspach EJ, Soveg F, Finn LS, So L, Gorman JA, Rosen ABI, Skoda-Smith S, Wheeler MM, Barrow KA, Rich LM, Debley JS, Bamshad MJ, Nickerson DA, Savan R, Torgerson TR, Rawlings DJ. Germline SAMD9L truncation variants trigger global translational repression. *J Exp Med* 2021;**218**:e20201195.
39. Shi H, O'Reilly VC, Moreau JL, Bewes TR, Yam MX, Chapman BE, Grieve SM, Stocker R, Graham RM, Chapman G, Sparrow DB, Dunwoodie SL. Gestational stress induces the unfolded protein response, resulting in heart defects. *Development* 2016;**143**:2561–2572.
40. Moreau JLM, Kesteven S, Martin E, Lau KS, Yam MX, O'Reilly VC, Del Monte-Nieto G, Baldini A, Feneley MP, Moon AM, Harvey RP, Sparrow DB, Chapman G, Dunwoodie SL. Gene-environment interaction impacts on heart development and embryo survival. *Development* 2019;**146**:dev172957.
41. Cerrone M, Remme CA, Tadros R, Bezzina CR, Delmar M. Beyond the one gene-one disease paradigm: complex genetics and pleiotropy in inheritable cardiac disorders. *Circulation* 2019;**140**:595–610.
42. Ittisoponpisan S, Alhuzimi E, Sternberg MJ, David A. Landscape of pleiotropic proteins causing human disease: structural and system biology insights. *Hum Mutat* 2017;**38**:289–296.
43. Geiler-Samerotte KA, Li S, Lazaris C, Taylor A, Ziv N, Ramjeawan C, Paaby AB, Siegal ML. Extent and context dependence of pleiotropy revealed by high-throughput single-cell phenotyping. *PLoS Biol* 2020;**18**:e3000836.
44. Paaby AB, Rockman MV. The many faces of pleiotropy. *Trends Genet* 2013;**29**:66–73.

45. Gottesman RF, Wu A, Coresh J, Knopman DS, Jack CR Jr, Rahmim A, Sharrett AR, Spira AP, Wong DF, Wagenknecht LE, Hughes TM, Walker KA, Mosley TH. Associations of vascular risk and amyloid burden with subsequent dementia. *Ann Neurol* 2022;**92**:607–619.
46. Miyake N, Takahashi H, Nakamura K, Isidor B, Hiraki Y, Koshimizu E, Shiina M, Sasaki K, Suzuki H, Abe R, Kimura Y, Akiyama T, Tomizawa S-I, Hirose T, Hamanaka K, Miyatake S, Mitsuhashi S, Mizuguchi T, Takata A, Obo K, Kato M, Ogata K, Matsumoto N. Gain-of-function MN1 truncation variants cause a recognizable syndrome with craniofacial and brain abnormalities. *Am J Hum Genet* 2020;**106**:13–25.
47. Lindholm ME, Jimenez-Morales D, Zhu H, Seo K, Amar D, Zhao C, Raja A, Madhvani R, Abramowitz S, Espenel C, Sutton S, Caleshu C, Berry GJ, Motonaga KS, Dunn K, Platt J, Ashley EA, Wheeler MT. Mono- and biallelic protein-truncating variants in alpha-actinin 2 cause cardiomyopathy through distinct mechanisms. *Circ Genom Precis Med* 2021;**14**: e003419.
48. Cioffi S, Flore G, Martucciello S, Bilio M, Turturo MG, Illingworth E. VEGFR3 modulates brain microvessel branching in a mouse model of 22q11.2 deletion syndrome. *Life Sci Alliance* 2022;**5**:e202101308.
49. Guo MY, Wang H, Chen YH, Xia MZ, Zhang C, Xu DX. N-acetylcysteine alleviates cadmium-induced placental endoplasmic reticulum stress and fetal growth restriction in mice. *PLoS One* 2018;**13**:e0191667.
50. Fra A, Yoboue ED, Sitia R. Cysteines as redox molecular switches and targets of disease. *Front Mol Neurosci* 2017;**10**:167.
51. Arbogast S, Ferreiro A. Selenoproteins and protection against oxidative stress: selenoprotein N as a novel player at the crossroads of redox signaling and calcium homeostasis. *Antioxid Redox Signal* 2010;**12**:893–904.
52. Lipinski P, Tylki-Szymanska A. Congenital disorders of glycosylation: what clinicians need to know? *Front Pediatr* 2021;**9**:715151.
53. Zhong C, Li P, Argade S, Liu L, Chilla A, Liang W, Xin H, Eliceiri B, Choudhury B, Ferrara N. Inhibition of protein glycosylation is a novel pro-angiogenic strategy that acts via activation of stress pathways. *Nat Commun* 2020;**11**:6330.
54. Patel C, Saad H, Shenkman M, Lederkremer GZ. Oxidoreductases in glycoprotein glycosylation, folding, and ERAD. *Cells* 2020;**9**:2138.
55. Schroeder AM, Nielsen T, Lynott M, Vogler G, Colas AR, Bodmer R. Nascent polypeptide-associated complex and signal recognition particle have cardiac-specific roles in heart development and remodeling. *PLoS Genet* 2022;**18**:e1010448.
56. Fontana F, Haack T, Reichenbach M, Knaus P, Puceat M, Abdelilah-Seyfried S. Antagonistic activities of Vegfr3/Flt4 and Notch1b fine-tune mechanosensitive signaling during zebrafish cardiac valvulogenesis. *Cell Rep* 2020;**32**:107883.
57. Karaman S, Leppanen VM, Alitalo K. Vascular endothelial growth factor signaling in development and disease. *Development* 2018;**145**:dev151019.
58. Marek-Iannucci S, Yildirim AD, Hamid SM, Ozdemir AB, Gomez AC, Kocaturk B, Porritt RA, Fishbein MC, Iwawaki T, Noval Rivas M, Erbay E, Arditi M. Targeting IRE1 endoribonuclease activity alleviates cardiovascular lesions in a murine model of Kawasaki disease vasculitis. *JCI Insight* 2022;**7**:e157203.
59. Weng KP, Cheng CF, Chien KJ, Ger LP, Huang SH, Tsai KW. Identifying circulating microRNA in Kawasaki disease by next-generation sequencing approach. *Curr Issues Mol Biol* 2021;**43**:485–500.
60. Persad KL, Lopaschuk GD. Energy metabolism on mitochondrial maturation and its effects on cardiomyocyte cell fate. *Front Cell Dev Biol* 2022;**10**:886393.
61. Ucar Z, Akbaba TH, Aydinoglu AT, Onder SC, Balci-Peynircioglu B, Demircin M, Balci-Hayta B. Mitochondrial dysfunction in cyanotic congenital heart disease: a promising therapeutic approach for the future. *Pediatr Cardiol* 2022;**43**:1870–1878.
62. Wang J, Zhang Y, Mendonca CA, Yukselen O, Muneeruddin K, Ren L, Liang J, Zhou C, Xie J, Li J, Jiang Z, Kucukural A, Shaffer SA, Gao G, Wang D. AAV-delivered suppressor tRNA overcomes a nonsense mutation in mice. *Nature* 2022;**604**:343–348.
63. Adachi H, Pan Y, He X, Chen JL, Klein B, Platenburg G, Morais P, Boutz P, Yu YT. Targeted pseudouridylation: an approach for suppressing nonsense mutations in disease genes. *Mol Cell* 2023;**83**:637–651.e9.
64. Helle E, Ampuja M, Dainis A, Antola L, Temmes E, Tolvanen E, Mervaala E, Kivela R. HiPS-endothelial cells acquire cardiac endothelial phenotype in co-culture with hiPS-cardiomyocytes. *Front Cell Dev Biol* 2021;**9**:715093.
65. Neri T, Hiriart E, van Vliet PP, Faure E, Norris RA, Farhat B, Jagla B, Lefrancois J, Sugi Y, Moore-Morris T, Zaffran S, Faustino RS, Zambon AC, Desvignes J-P, Salgado D, Levine RA, de la Pompa JL, Terzic A, Evans SM, Markwald R, Pucéat M. Human pre-valvular endocardial cells derived from pluripotent stem cells recapitulate cardiac pathophysiological valvulogenesis. *Nat Commun* 2019;**10**:1929.
66. Mikryukov AA, Mazine A, Wei B, Yang D, Miao Y, Gu M, Keller GM. BMP10 signaling promotes the development of endocardial cells from human pluripotent stem cell-derived cardiovascular progenitors. *Cell Stem Cell* 2021;**28**:96–111.e7.
67. Saha P, Potiny P, Rigdon J, Morello M, Tcheandjieu C, Romfh A, Fernandes SM, McElhinney DB, Bernstein D, Lui GK, Shaw GM, Ingelsson E, Priest JR. Substantial cardiovascular morbidity in adults with lower-complexity congenital heart disease. *Circulation* 2019;**139**: 1889–1899.
68. Byrne DJF, Williams SG, Nakev A, Frain S, Baross SL, Vestbo J, Keavney BD, Talavera D. Significantly increased risk of chronic obstructive pulmonary disease amongst adults with predominantly mild congenital heart disease. *Sci Rep* 2022;**12**:18703.